Dosage-dependent antimicrobial activity of DNA-histone microwebs against *Staphylococcus aureus*

Ting Yang, Shi Yang, Tasdiq Ahmed, Katherine Nguyen, Jinlong Yu, Xuejun Cao, Rui Zan, Xiaonong Zhang, Hao Shen, Meredith E Fay, Evelyn Kendall Williams, Wilbur A. Lam, J. Scott VanEpps, Shuichi Takayama,* Yang Song*

T. Yang, Prof. X. Cao
State Key Laboratory of Bioreactor Engineering, Department of Bioengineering, East China University of Science and Technology, Shanghai 200237, China.

T. Yang, T. Ahmed, K. Nguyen, M. E. Fay, E. K. Williams, Prof. W. A. Lam, Prof. S. Takayama

Wallace H Coulter Department of Biomedical Engineering & Petit Institute for Bioengineering and Bioscience, Georgia Institute of Technology & Emory School of Medicine, Atlanta, GA 30332 USA.
E-mail: takayama@gatech.edu

S. Yang, R. Zan, Prof. X. Zhang, Dr. Y. Song

State Key Laboratory of Metal Matrix Composites, School of Material Science and Engineering, Shanghai Jiao Tong University, Shanghai 200240, China.
E-mail: nanosurface@sjtu.edu.cn

J. Yu, Prof. H. Shen
Department of Orthopedics, Shanghai No.6 People's hospital, Shanghai 200233, China.

Prof. J. S. VanEpps

Department of Emergency Medicine, Michigan Center for Integrative Research in Critical Care, Biointerfaces Institute, University of Michigan, Ann Arbor, MI 48109 USA.

Abstract

Neutrophil extracellular traps (NETs) is an antimicrobial cobweb-structured material produced by immune cells for clearance of pathogens in the body, but paradoxically associated with biofilm formation and exacerbated lung infections. To provide a better materials perspective on the pleiotropic roles played by NETs at diverse compositions/concentrations, a NETs-like material (called 'microwebs', abbreviated as µwebs) is synthesized for decoding the antimicrobial activity of NETs against *Staphylococcus aureus* in infection-relevant conditions. We show that µwebs composed of low-to-intermediate concentrations of DNA-histone complexes successfully trap and inhibit *S. aureus* growth and biofilm formation. However, with growing concentrations and histone proportions, the resulting microwebs appear gel-like structures accompanied by reduced antimicrobial activity that can even promote formation of *S. aureus* biofilms. Our simplified model of NETs provides a materials-based evidence on NETs-relevant pathology in the development of biofilms.

1. Introduction.

Biofilms are surface-bound microbe assemblies encased in extracellular matrix including eDNA, proteins and polysaccharides, which allow bacteria to resist host immune clearing

mechanisms.[1] One critical biofilm component is eDNA, which helps maintain biofilm structural integrity,[2] as well as counter host antimicrobial peptides[3] and antibiotic treatments.[4] Although eDNA can engage positively with pathogens, it is known to have an important role in the innate immune response, where neutrophils may be triggered to release neutrophil extracellular traps (NETs),[5, 6] cobweb-structured DNA-histone complexes that capture and disarm microorganisms.[7, 8] The observed antimicrobial activity of NET-based eDNA is due, at least in part, to their chelation with bacterial membrane proteins and subsequent lysis.[9] Histones, key NET components that modulate the self-assembly of DNA, also contribute to overall antimicrobial activity by destabilizing bacterial cell walls and chromosome organization.[10, 11] It is also reported that histone inhibits biofilm formation in a dosage-dependent manner.[12] Previous studies have indicated that the antimicrobial activity of DNA or histone largely depend on their surface charges, and blockage of the surface charge results in declined antimicrobial activity.[9, 11]
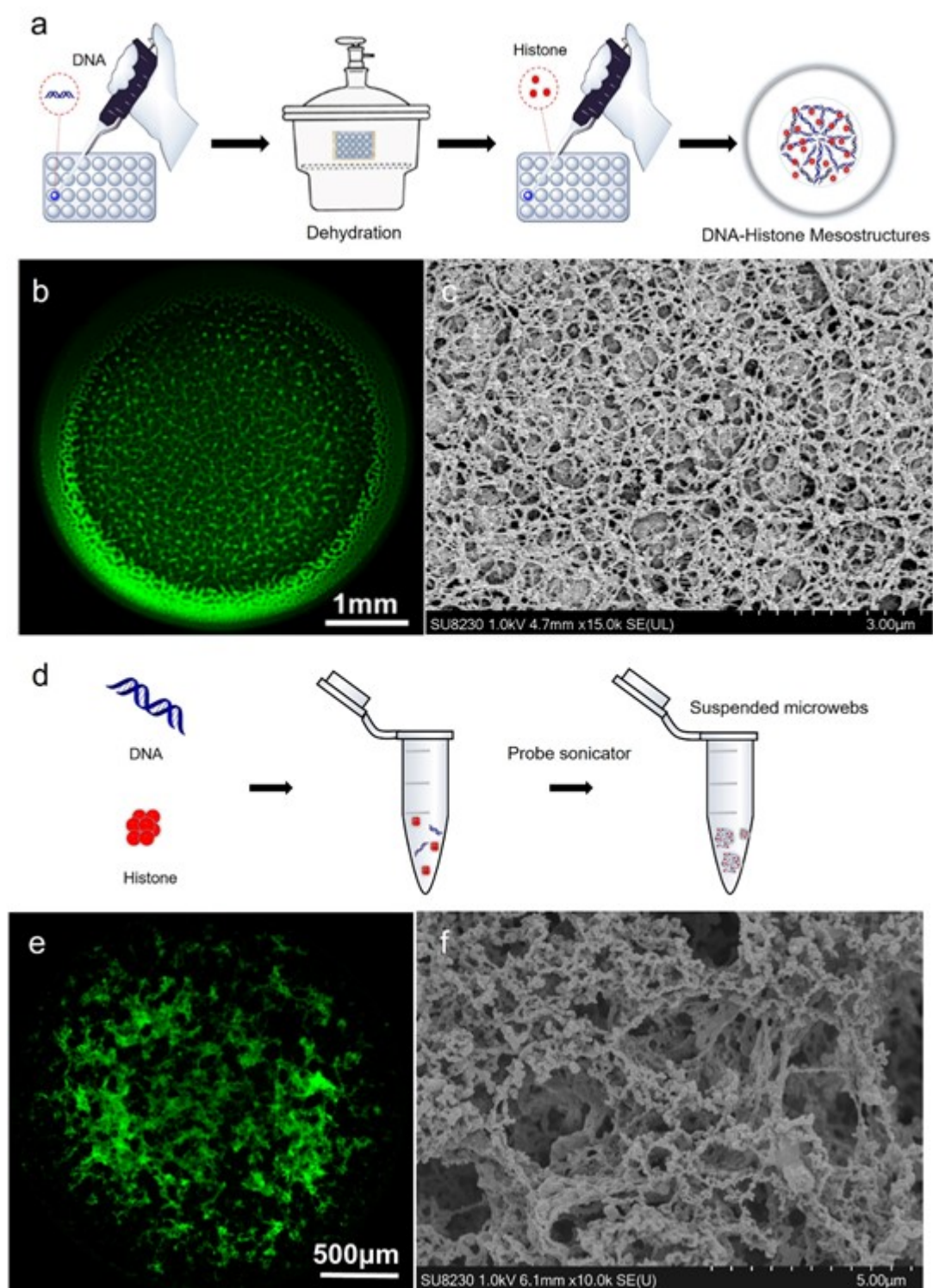
Staphylococcus aureus is an opportunistic pathogen that can cause persistent biofilm infections in soft tissues and bones.[13] Planktonic *S. aureus* induces neutrophils to produce NETs that can effectively trap and suppress the bacteria.[7] On the other hand, *S. aureus* biofilms can thwart the antimicrobial functions of NETs by secreting nucleases to degrade the eDNA in NETs;[5, 14, 15] they also utilize fibronectin-binding protein B (FnBPB) and proteases to neutralize histone-mediated killing.[10, 16] Producing DNA-degrading nucleases that protect

3

them from NETs within hours of surface-attachment,[5] *S. aureus* biofilms actively induce

neutrophil NETosis to protect themselves from other granulocytic killing mechanisms.[17]

In contrast to the many studies that study how biofilms affect neutrophils, NETosis, and

NETs, there is no systematic analysis of how different types of NETs may impact planktonic

S. aureus response in forming biofilms. This may be important because NET composition

including protein content and DNA sources has been previously found to vary depending on

the NETosis stimulant.[18] Additionally, there may be relevant, physiological composition

changes that occur over time as DNases and proteases selectively degrade NET components

to skew component ratios.[5, 10, 15-17] We have previously demonstrated preparation of

DNA-histone μwebs with NETs-like structures and antimicrobial functions.[19] Unlike NETs

collected from activated neutrophils, μwebs can be compositionally well-defined in order to

facilitate the systematic evaluation of component-specific biological effects. Here, we

evaluate how different concentrations and ratios of the main NET components, DNA and

histone, induce or suppress *S. aureus* biofilm formation.

2. Results and Discussion

DNA-histone complexes constitute the backbone of endogenous NETs, and the mass ratio of

DNA to histone in the as-formed NETs is close to 1:1.[20] By mimicking the structure,

composition and antimicrobial function of NETs backbone, we have previously reported that

DNA-histone μweb suspensions inhibit proliferation of Gram-negative *E. coli* in a DNA:

histone ratio-dependent manner[19] and that DHMs stimulate proinflammatory responses from dendritic cells.[21] DHMs form a stable and intact membrane coated on the microwell plates, which can withstand flushing by manual pipetting, as described in **Figure 1a**. By staining with SYTOX green, the DNA backbone in the DHMs is visualized as a porous mesh (Figure 1b); SEM images (Figure 1c) show that the DNA mesh pore size is approximately 50-300 nm. The μwebs with the same concentration of DNA and histone as DHMs were prepared by homogenization in HBSS using a probe sonicator (Figure 1d). These μwebs are colloidal suspensions with a size distribution similar to the endogenous NETs collected from neutrophils. Fluorescent microscopy (Figure 1e) and scanning electron microscopy (Figure 1f) reveal that surface-adsorbed μwebs show similar DNA-rich structures with their pore sizes varied from 20 to 100 nm, in agreement with that observed on the NETs. These mesh-like structures with submicron sized pores enables entrapment of bacteria that have characteristic lengths of 0.4 ~ 2 μm.

a

DNA

Dehydration

Histone

DNA-Histone Mesostructures

b

1mm

c

SU8230 1.0kV 4.7mm x15.0k SE(UL)   3.00μm

d

DNA

Histone

Probe sonicator

Suspended microwebs

e

500μm

f

SU8230 1.0kV 6.1mm x10.0k SE(U)   5.00μm

Figure 1. Preparation and characterization of DHMs and microweb (μweb) suspensions. (a) Schematic showing the preparation of a DHM from dehydrated DNA-rich droplets. (b) A fluorescent image of the DHM membrane, showing DNA (green) resembles into a mesh in the DHMs overall structure. (c) SEM observation of mesh-like DHMs with submicron pores. (d) Preparation of μweb suspensions. (e) Fluorescence microscopy image of surface-bound μwebs. (f) Scanning electron microscopy image of surface-bound μwebs.

Bacterial adhesion on a surface is often a prerequisite for biofilm formation.[22] Considering many NET structures may be surface bound while others are floating in body fluids, we tested bacterial adhesion on two forms of DNA-histone structures, including DHMs and μwebs with the same formulations (Figure 2e & S1). Using GFP-*S. aureus*, we seeded 10^7 cells into DHM-coated 96-well plates (tissue culture-treated, polystyrene), using nutrient-poor HBSS media. Uncoated, DNA or histone coated microwells were used as control groups. The total weight of DNA or histone solution in each well was equal to that used for forming the DHMs. After incubation for specified periods (0.5, 1.5 and 4.5 hours), we aspirated the unattached/loosely attached bacteria by washing the microwells with HBSS three times; the number of attached bacteria was quantified from their relative fluorescence intensity (RFI). In the first half hour, only weak RFI signal was detected from all groups, suggesting that the time interval was too short for bacteria to adhere or that the substrate attachment of *S. aureus* was weak, reversible, and readily washed away at the beginning. After 1.5 hours, the number of attached bacteria was drastically increased on the

7

DHM-coated substrate compared to that in the non-coated microwells, as shown in Figure 2a & b. Measurements of the bacterial RFI suggest that 50-100 times more cells were adhered to the DHM-coated substrate than to the non-coated substrate. The DNA or histone-coated microplates did not induce pronounced adhesion of *S. aureus* in the first 1.5 hours. By staining the eDNA and dead bacteria with propidium iodide, three-dimensional fluorescent images (Figure 2c & d) of DHMs and trapped bacteria could be constructed using CLSM. We found that only a small fraction (<10%) of the attached *S. aureus* had died, while the majority of surface-attached *S. aureus* (>80%) aggregated into clusters after being trapped on the DHM. At t = 4.5 hours, the number of live bacteria attached to the non-coated, DNA-containing and histone-containing microwells started to increase, and the RFI of *S. aureus* in the DHM-coated microplates remained stable at a high level (Figure 2e). When μwebs were used for the bacterial adhesion test, we also observed more bacterial adhesion on the μwebs than that in the DNA or histone groups (see Figure S1).
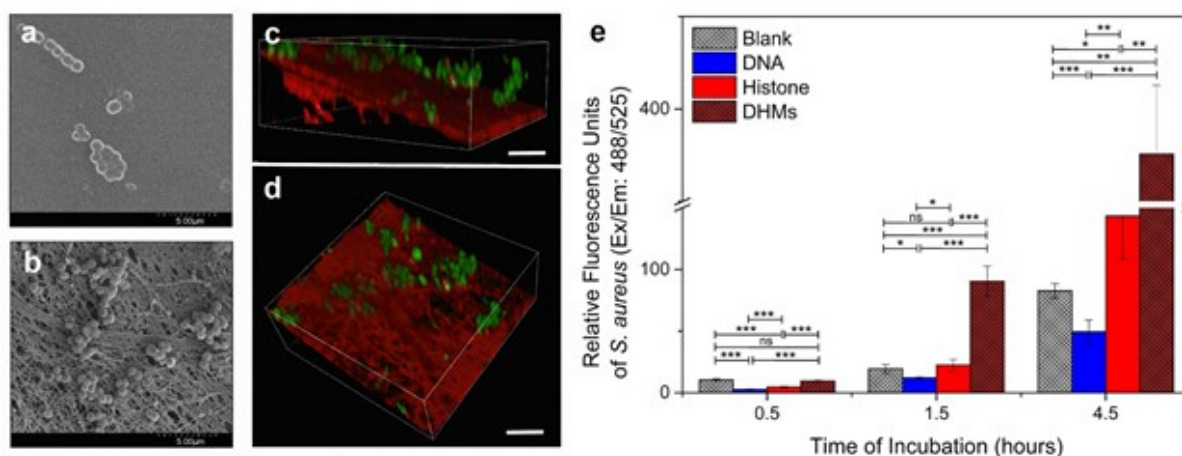
Figure 2. DNA-histone mesostructures (DHMs) promote adhesion of *S. aureus* in nutrient poor HBSS medium. (a,b) SEM images showing the adhesion of *S. aureus* on a) non-coated and b) DHM-coated substrates. t =1.5 hour. (c,d) CLSM 3D reconstructions showing the attached *S. aureus* aggregate into small clusters. Red: propidium iodide stained DHM and dead *S. aureus*; Green: live *S. aureus*. t =1.5 hour. (e) Statistics of the relative fluorescence intensity of *S. aureus* attached to non-coated, DNA-coated, histone-coated, or DHM-coated microplates. The statistics were performed by ANOVA with post hoc Tukey test: ns, not significant; *$p < 0.05$, **$p < 0.01$ and ***$p < 0.001$, N=6 for each condition.

Having compared bacterial adhesion on surface-attached DHMs (Fig 2) and µwebs (Fig S1), we pursued further studies with the more conveniently handled DNA-histone µweb suspensions. We have previously reported that DNA-histone µweb suspensions that possess a positive zeta potential are antimicrobial materials against Gram-negative *E. coli* due to the bactericidal activity of histone, which can permeabilize the bacterial cell wall.[19] Here, µweb- and histone-induced bactericidal activity is observed with *S. aureus*, as shown by the reduced CFU counts after culturing *S. aureus* with 200 µg mL^{-1} histone solution in nutrient-poor HBSS media for 1.5 hours (Figure 3a). When cultured in the commonly used, nutrient-rich TSBg medium, histone remains efficient in killing *S. aureus* while DNA alone minimally inhibits proliferation of *S. aureus* (Figure 3b & c). Although µweb presented antimicrobial activities against *S. aureus* under these conditions, the antibacterial potency of histones is compromised after binding with DNA (Figure 3d).[23] We also conducted experiments with two different strains of bacteria (RN4220 versus US300) in two different labs (Shanghai and

9

Atlanta). The µweb effects were somewhat different against RN4220 (Figure 3d) versus US300 (see Figure S2). Because the source of DNA, histones, and media components may be somewhat different depending on the lab and location, caution is required in making strong conclusions, but the RN4220 strain had a more complex concentration-dependent response to the antimicrobial activities of DNA and µwebs. We thus proceeded with additional µweb dosage experiments using the RN4220 strain.
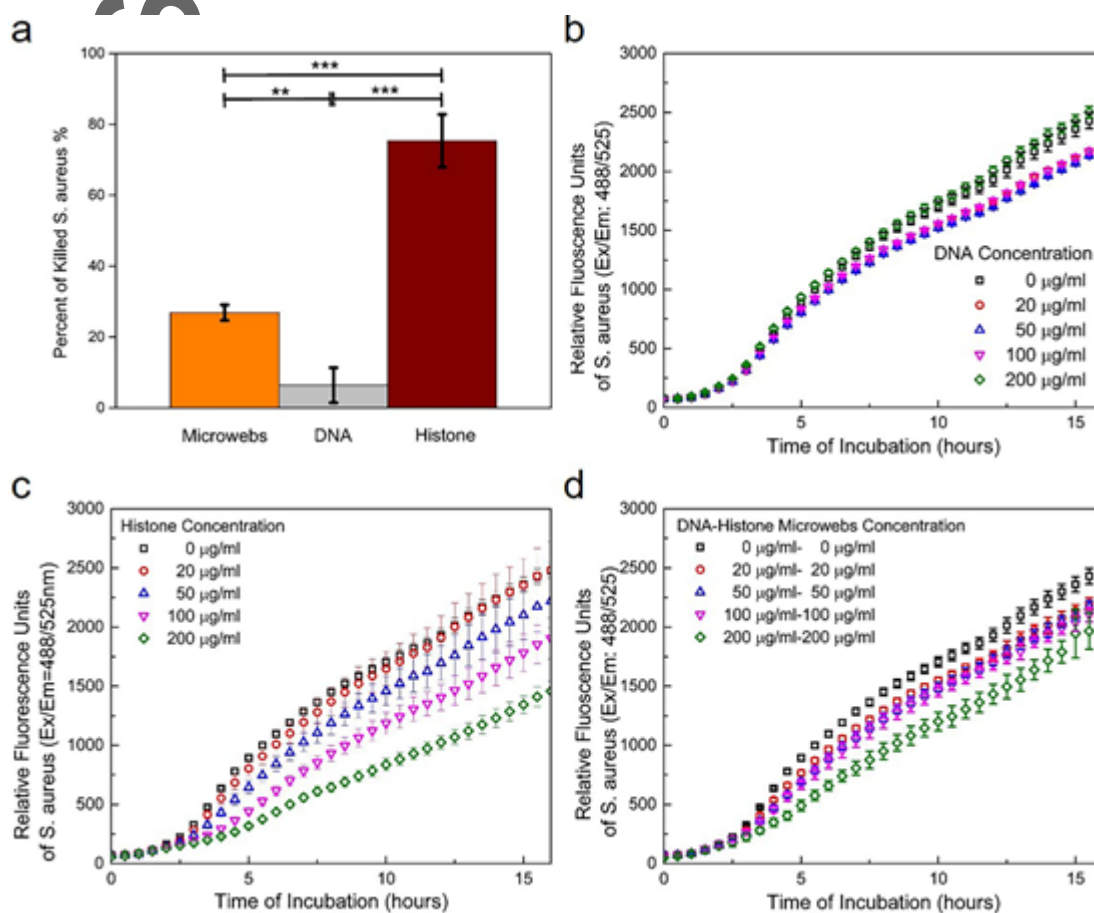

Figure 3. Evaluation of the bacterial killing potency of DNA, histone and DNA-histone µweb suspensions against *S. aureus*. a) Enumeration of colony forming units of *S. aureus* (seeding density: 10^6 CFU mL^{-1}) after culture in nutrient-poor HBSS media, DNA-histone

µwebs suspensions (200 µg mL^{-1} DNA + 200 µg mL^{-1} histone), DNA solution (200 µg mL^{-1}) and histone solution (200 µg mL^{-1}). ANOVA followed by Tukey's test was used for statistical analysis: ns, not significant; *p < 0.05, **p < 0.01 and ***p < 0.001, N=6 for each condition. b-d) Growth curves of *S. aureus* in nutrient-rich TSBg medium containing (b) eDNA, (c) histone, or (d) µwebs at physiologically relevant concentrations. Seeding density: 10^7 CFU mL^{-1}.

The formation of biofilms on polystyrene surfaces from suspensions of bacteria with and without µwebs was visualized at different time points under SEM, as shown in Figure 4a-c. During the first 6 hours of incubation, *S. aureus* were trapped in the meshwork of µwebs and a subset of bacteria had their cell wall damaged, likely resulting from histone-mediated bacterial killing. In comparison, the *S. aureus* in µweb-free medium remained intact during the initial 6 hours (Figure 4d). At t=12 hours, more *S. aureus* were lysed after being trapped in µwebs,[7] and the intracellular compounds released from dead bacteria entangled with the µweb meshwork (Figure 4b). In contrast, little bacterial extracellular polymeric substances (EPS) were deposited in µweb-free culture (Figure 4e). The antimicrobial activity of the µweb is typically insufficient to kill all *S. aureus*; instead, most *S. aureus* continue to proliferate and form biofilm with more EPS after 24 hours (Figure 4c) compared with the µweb-free control group (Figure 4f). These observations suggest that µwebs may play an important role in the formation of early-stage biofilm.[24]
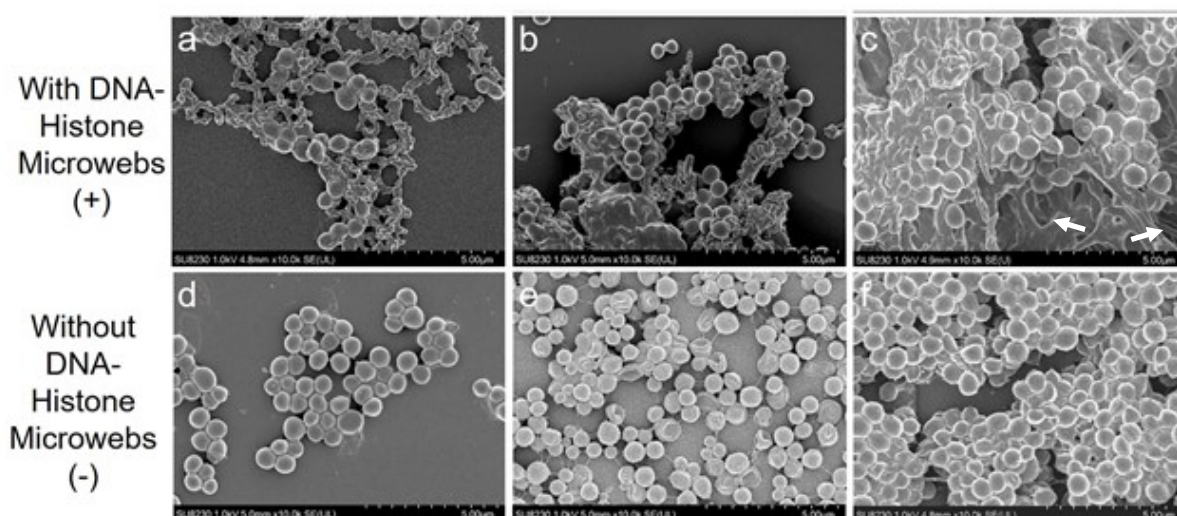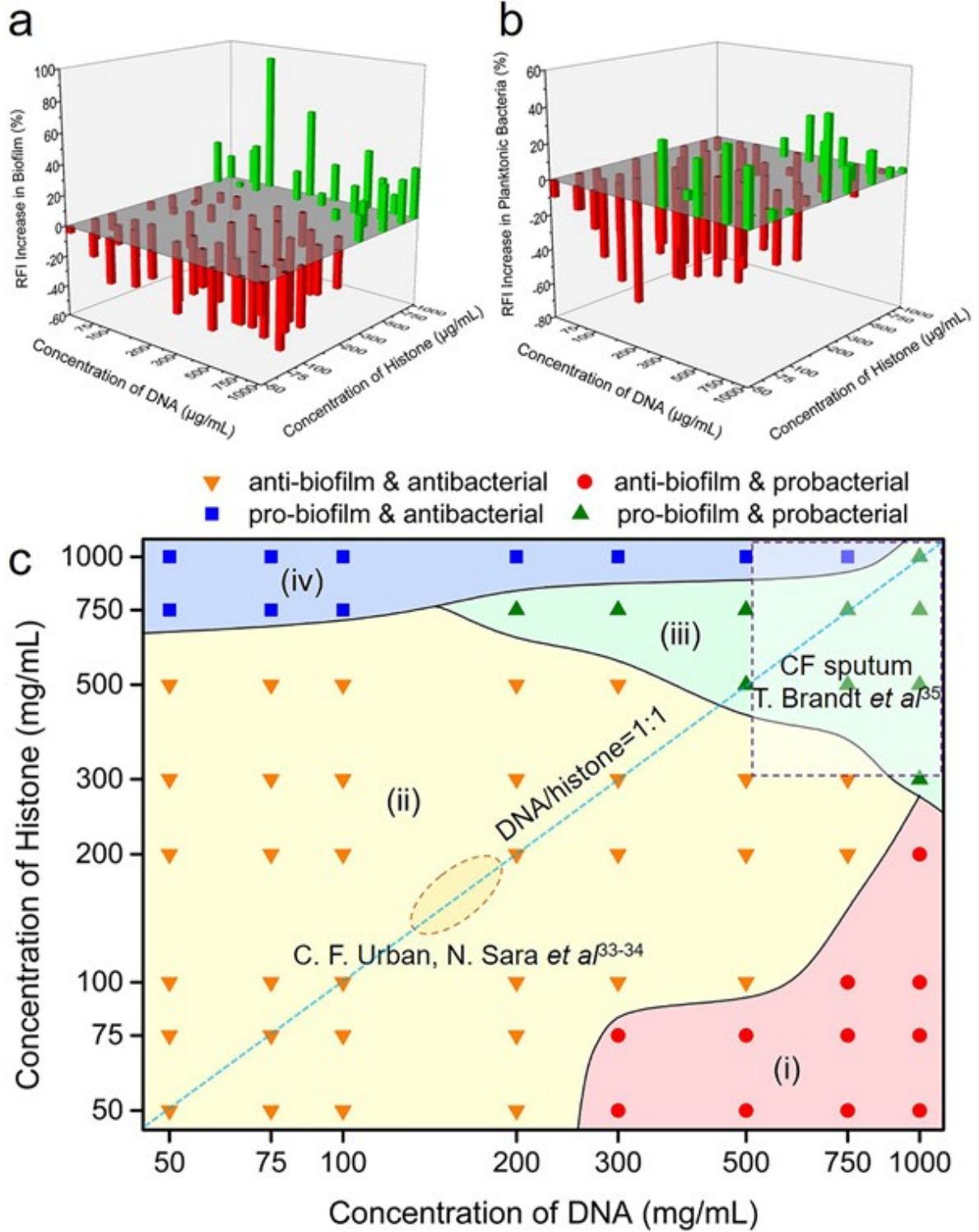
11

Figure 4. Aggregated clumps of μwebs promote formation of *S. aureus* biofilm in nutrient rich TSBg medium. (a-c) SEM images showing that 400 μg mL^{-1} μweb promotes formation of *S. aureus* biofilm. Time of bacterial incubation, (a) t=6hr, (b) t=12hr, (c) t=24hr. The white arrows indicate the EPS or bacteria lysed by μweb. (d-f) SEM images showing formation of *S. aureus* biofilm without addition of μwebs in the culture medium. (d) t=6hr, (e) t=12hr, (f) t=24hr.

To further understand how the composition of μwebs alters the bacterial mode of growth between the planktonic and biofilm states, *S. aureus* were cultured in TSBg supplemented with μwebs prepared from mixtures of DNA (0-1000 μg mL^{-1}) and histone (0-1000 μg mL^{-1}) at different concentrations (Figure 5). After incubation for 24 hours, the floating *S. aureus* in the supernatant were transferred to a new microplate while the wells containing the surface-attached biofilms were refilled with HBSS. The relative fluorescence intensity (RFI) of GFP-*S. aureus* in the biofilm (I_b) and that in the supernatant (I_s) were separately quantified using a plate reader. As a blank control group, *S. aureus* were cultured in μweb-free medium for 24 hours, and the RFI in the biofilm (I_{b0}) and in the supernatant (I_{s0}) were recorded

separately. Compared to the blank control group, formation of biofilm in the presence of

μwebs is either increased if $I_b > I_{b0}$, or decreased if $I_b < I_{b0}$. The increases in the RFI in the

biofilm amount relative to the μweb-free group is calculated by $(I_b-I_{b0})/I_{b0}$, as shown in Figure

5a. Meanwhile, the number of planktonic *S. aureus* is either increased if $(Is-Is_0)/Is_0 > 0$, or

decreased if $(Is-Is_0)/Is_0 < 0$ (Figure 5b).

a

b

c

- ▽ anti-biofilm & antibacterial
- ● anti-biofilm & probacterial
- ■ pro-biofilm & antibacterial
- ▲ pro-biofilm & probacterial

Figure 5. Concentration-dependent antimicrobial/biofilm promoting effects of μwebs on *S. aureus*. *S. aureus* were cultured with μwebs for 24 hours to evaluate the effect of μwebs with different compositions on the formation of *S. aureus* biofilm. The RFIs of planktonic bacteria and biofilm were measured separately. a) Changes in the RFIs of *S. aureus* biofilm in the presence of μwebs with different compositions. b) Changes in the RFIs of the planktonic *S. aureus* in the presence of μwebs with different compositions. c) A state diagram showing the effect of μweb compositions on the mode of bacteria growth in TSBg. Four different regions are defined in the diagram: (i) red, inhibits the formation of biofilm and slightly promotes growth of planktonic bacteria. (ii) yellow, inhibits both growth of biofilm and planktonic bacteria. (iii) green, promotes the growth of planktonic bacteria and formation of biofilm. (iv) blue, inhibits the growth of planktonic bacteria but prompts biofilm formation. The solid lines dividing boundaries between different zones are served as a guide for the eye.

By varying the formulations of μwebs and measuring the changes in RFI in the biofilm and in the supernatant relative to that in the blank control group, we obtain a diagram to describe four different categories of bacterial growth in the presence of μwebs, as shown in Figure 5c. When the DNA/histone weight ratio approaches that of endogenous NETs, $W_{(DNA)}:W_{(histone)} = 1:1$, the μwebs inhibit the growth of both floating bacteria and biofilm only if the DNA concentration is below a critical value 500 μg mL^{-1} (yellow region).[19, 25] Above this critical concentration, the μwebs were observed to form hydrogels (see Figure S3) and their antimicrobial function diminished. Instead, formation of biofilm is accelerated under this condition (as shown by the green region in Figure 5c), probably because the probably because the μwebs with a relatively high DNA concentration serve as nutrient reservoirs for both biofilm and planktonic bacteria growth.[26] Previous studies have reported that eDNA

15

can associate with positively-charged bacterial matrix proteins in a low-pH environment, thereby supporting biofilm formation.[27] Similarly, we find that the complex of eDNA and histone promotes bacterial adhesion (see Figure 2e) and biofilm formation (Figure 5c) at relatively high concentrations.

When the total concentration of μwebs is maintained constant, an increasing weight ratio of DNA/histone (as shown by the red region in Figure 5c) tends to reduce the settling of *S. aureus* and formation of biofilm. The μwebs with relatively low weight ratios of DNA/histone promote biofilm formation (blue region) and decrease the number of planktonic *S. aureus*. This apparent μweb-mediated formation of biofilm may be explained by the interaction between bacteria and the μweb electrostatic meshwork. Many polycationic polymers and peptides, such as polyethyleneimine (PEI) and cathelicidin LL-37 relies on their positive surface charges to target and penetrate through the bacterial cell wall.[28] Among structurally similar molecular entities, antimicrobial copolymers with higher zeta potentials typically have more potent bactericidal activity than those with lower zeta potentials.[29] In consistency with these observations, our experiments show that the antimicrobial activity of bactericidal histone is declined after combining with NET DNA (Figure 3c).[19, 29] The number of floating bacteria decreases as the fraction of histone in μwebs increases, likely for two reasons: either histone facilitates killing of planktonic *S. aureus*, and/or the histone-induced environmental stress promotes conversion from

16

planktonic state to biofilm. Adhesion of *S. aureus* on µwebs decreases as the DNA fraction in the µwebs increases, probably driven by the growing electrostatic repulsion between bacterial matrix proteins and DNA phosphate backbones, which in turn attenuates the antimicrobial potency of µwebs against floating bacteria.

The model of electrostatic interactions between µwebs and *S. aureus* is further supported by our zeta potential measurements. After the DNA (ζ = -55.9 ± 2.4 mV) and histone (ζ = +11.6 ± 0.3 mV) solutions are mixed to form µweb suspension, the zeta potential of resultant µwebs increases with the growing histone fraction (see Figure S4).[19] With sufficiently high zeta potentials (≥9 mV) and histone concentrations (≥500µg/ml), planktonic *S. aureus* were easily killed. With sufficiently low zeta potentials (≤-20 mV) and high DNA concentrations (≥300µg/ml), formation of *S. aureus* biofilm was suppressed. When the zeta potentials of µwebs fall between -20 mV and 9 mV, the bactericidal activity of µwebs largely depends on their degree of gelation (see Figure S3). At a fixed mass ratio of DNA to histone, an increase in the concentration of DNA and histone causes stronger aggregation of hydrocolloids, resulting in lower membrane permeability across the bacterial cell wall.[19] Consequently, the µwebs with NETs-like compositions (DNA: Histone=1:1) allow bacterial trapping and clustering but fail to eliminate *S. aureus* efficiently at a high physiological concentration (500-1000 µg mL^{-1}). These findings support the hypothesis that the electrostatic interaction between DNA, histone and *S. aureus* impact the bacterial clustering, colonization and the

17

subsequent assembly of biofilms. A schematic showing how NETs compositions affect *S. aureus* biofilm formation and the proposed mechanism is summarized in Figure 6.
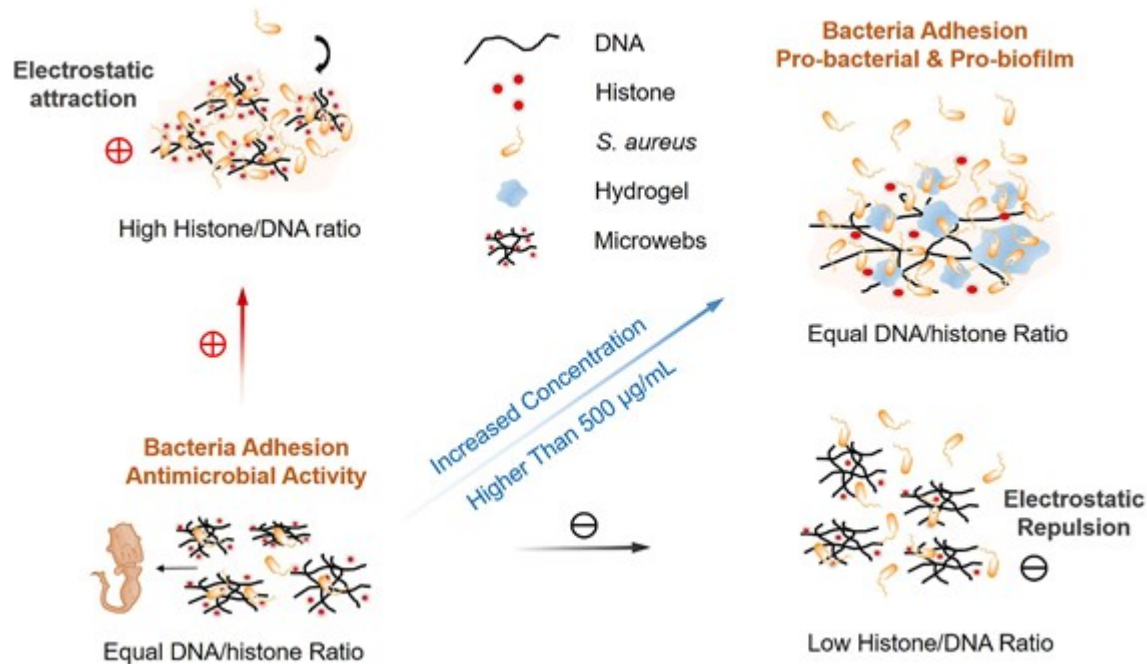

Figure 6. A schematic illustration of the S. aureus responses to µwebs with varying compositions.

The dose-dependent antimicrobial and pro-biofilm properties of µwebs may shed lights on understanding the pleiotropic roles of NETs. Most endogenous NETs have a DNA/histone weight ratio close to 1:1 (see the dotted blue line in Fig.5c), and their physiological concentrations typically fall within 400 µg mL^{-1}[25, 30] (denoted by the dotted ellipse), so NETs exhibit antimicrobial activity against planktonic bacteria and biofilms in general immune responses. However, NETs can cause obstruction of airways in cystic fibrosis (CF)

patients, and the DNA concentration in their sputum and bronchoalveolar lavage fluids goes

over 600 µg mL^{-1}[31] (denoted by rectangle in Fig.5c). Many clinical studies have reported

that a high DNA level in airway fluids strongly correlates to the exacerbation of CF lung

infection.[32] Our phase diagram indicates that the gelatinous microwebs formed by

concentrated DNA/histone become malfunctional antimicrobial structures and pathologically

relevant to the exacerbation of *S. aureus* infection. The aggregation of µwebs colloids and

their gelation at high DNA and histone concentrations may result in declined permeability

across bacterial wall and reduced bactericidal potency. We have previously reported that

dosage-dependent antimicrobial activity of µwebs against *E.coli UTI89*.[19] *E. coli* with

thinner bacterial cell wall than *S. aureus* are more susceptible to the histone-mediated killing,

suggesting the permeability of polycationic histone across the bacterial cell wall is critical to

their antimicrobial activity. However, responses of Gram negative bacteria to the µwebs

could be very complicated and unexplored. E.g, *E. coli* were observed to elongate in response

of µweb-mediated killing, rather than forming biofilm.[19] These observations suggest many

differences in bacterial responses to NETs, depending on different bacterial strains, which

deserve further investigations.

3. Conclusions

In summary, we synthesized DHMs and µweb suspensions with NET-like structures for
understanding the role of the overall material dosage, with different zeta potentials, in the
development of *S. aureus* biofilms. Microwells coated with DHMs promote fast and efficient

trapping (or adhesion) of *S. aureus,* compared to microwells coated with polyanionic DNA or bactericidal histone. Although DNA or histone alone are thought to be antimicrobial, the antimicrobial potency of suspended μwebs varies with their concentration. Interestingly, high concentrations of μwebs that lead to formation of gel-like bacteria-clusters promote bacterial growth and biofilm formation, and μwebs with relatively low DNA/histone ratios promote bacterial clustering and biofilm formation. Our analysis provides improved understanding of how NET components might impact *S. aureus* viability and biofilm formation. Further studies need to confirm the generalizability of our observations by testing different clinical isolates of bacterial strains. While neutrophils may not produce NETs with such drastically varied compositions as studied in this paper, there may be relevant, physiological composition differences as well as changes that occur over time as DNases and proteases selectively degrade NET components to skew component ratios.[5, 14, 17] There are multiple clinical situations where high concentrations of NETs components are present physiologically such as in cystic fibrosis[31] and soft tissue infections.[33] The data from our study is envisioned to assist in the development of hypotheses for future biological and pathological studies of how NETs and biofilms may exacerbate or alter the course of infections.

4. Experimental Section

Preparation of DHMs: To mimic attached NETs, DNA-histone mesostructures (DHMs) were

prepared by ionic crosslinking of salmon DNA (salmon DNA, Sigma, D1626) using calf

thymus histone (Diamond, A002544-0250) in the presence of trehalose dihydrate (Beyotime,

ST1245).[21] Firstly, salmon DNA was dissolved into 0.4M trehalose solution until the final

DNA concentration reached 150 μg mL^{-1}. Next, 40 μL of DNA-trehalose solution was

spotted to the center of each well of a 96-well plate (Tissue culture treated, BWTC). After

vacuum drying in a desiccator for 24 hours, the dehydrated DNA-trehalose forms a glassy

film. Next, 60 μL of histone solution (0.1 μg mL^{-1}, dissolved in 0.1M Tris-HCl, pH=8) was

added into each well to rehydrate the DNA-trehalose film. After incubation for 3 hours, a

20

thicker, fibrous, DHMs formed. Trehalose was dissolved and removed upon washing with deionized water three times.

Preparation of suspended μwebs: To mimic NETs in suspension, suspended μwebs were produced by mixing DNA and histone together at different concentrations and ratios, followed by using a probe sonicator (Qsonic 125, intensity set: 20%, 15 seconds) to homogenize the mixture in Hank's Balanced Salt Solution (HBSS) solutions.

Characterization of surface-bound DHMs and μwebs: DHMs or μwebs were stained with 0.01% SYTOX green (Sigma) or 0.5 vol% propidium iodide (Sigma) solution for 15 minutes, washed repeatedly and observed under a fluorescent microscope (Nikon Eclipse 80i). The surface-bound DHM and μweb structures were also observed by scanning electron microscopy (SEM, Hitachi SU8230). In brief, samples were fixed in 4% paraformaldehyde for 30 mins, washed with deionized water, and sequentially dehydrated in 25 vol%, 50 %, 75 %, 95 %, and 100 % ethanol respectively. After ethanol dehydration, the structures were immersed in hexamethyldisilane and vacuum-dried overnight. The next day, the sample was sprayed with gold nanoparticles using a modular sputter coater (SPI-Module 60s, 18 mA). Scanning electron microscopy[34] images of the samples were taken under the following condition: Ucc = 1 kV, I = 15 mA.

Bacteria culture: A frozen glycerol stock of *S. aureus*[35] (strain RN4220-sfGFP transfected with GFP plasmid, China) was streaked on a tryptic soy agar (TSA, Sigma 22091) plate and

21

incubated at 37 °C. After overnight culture, one bacterial colony was scratched from TSA

plate and suspended in 1 mL tryptic soy broth (TSB, Sigma 22092) supplemented with 1wt%

glucose (TSBg). The bacteria culture was further incubated under a rotation speed of 220 rpm

at 37 °C for 3-4 hours until their optical density OD_{600} reaches 0.3~0.6. Then, the culture is

diluted using TSBg until $OD_{600} = 0.02$ (*S. aureus* density: ~10^7 CFU mL^{-1}) for bacterial

adhesion and growth curve measurement. For a subset of tests (see SI), we also used a

different methicillin-resistant *S. aureus* with GFP label (strain USA300).[36]

Bacterial adhesion test: 10^7 *S. aureus* cells (counted in Colony Forming Units, CFU)

pre-suspended in 200 µL of HBSS were seeded into DHM-coated 96-well plates. As a blank

control, an equal number of bacteria suspended in HBSS were seeded into DHM-free 96-well

plates. To understand the contribution of the individual NET components to bacterial

adhesion, the HBSS was supplemented with DNA or histone before dispensing into

non-DHMs-coated 96-well plates for comparison. The total weight of DNA or histone in the

µwebs was prepared equally to that in the DHMs of the experimental group. After incubation

for 0.5-4.5 hours, the unattached bacterial cells were extracted by pipetting and the remaining

S. aureus were washed with HBSS twice. The amount of live bacteria attached to the

microwell plates was quantified from the relative GFP fluorescence intensity using a plate

reader (Biotek Synergy HT). One-way analysis of variance (ANOVA) followed by post-hoc

Tukey test was applied to quantify statistical significance. Dead *S. aureus* attached to the

DHMs were stained by using 0.5 vol% propidium iodide solution and observed under a confocal laser scanning microscope.[37]

Zeta potential measurement: The zeta potentials of *S. aureus* incubated with suspended μwebs or its separate components (DNA or histones) were measured using a zeta potential analyzer (Nanobrook Omni).[38] Bacteria cultures (OD_{600} = 0.02) were centrifuged at 12,000g for 10 min. Thereafter, the supernatant was discarded, and the bacterial pellet was resuspended in 1 mL HBSS or HBSS supplemented with DNA, histone, or μwebs at different concentrations of 50, 100 and 200 μg mL^{-1}. The samples were incubated at 37 °C for 0.5 hour before their zeta potentials were measured.

Bacterial killing test: 10 μL of *S. aureus* culture (OD = 0.02) were separately mixed with 100 μL HBSS, HBSS supplemented with DNA (200 μg mL^{-1}), HBSS supplemented with histone (200 μg mL^{-1}) and HBSS supplemented with suspended μwebs (400 μg mL^{-1}, the DNA: histone weight ratio= 1:1). After 1 h incubation at 37°C, the bacterial culture was diluted with deionized water at a ratio of 1:1000. Subsequently, 10 μL of the diluted bacterial culture was extracted and spotted on a tryptic soy agar plate. Each sample was serially diluted 6 times to obtain a minimum of 50 CFU counts in the blank control group. After further incubation overnight, the CFU counts in each bacterial sample were enumerated, presented as mean values ± S.D. The percent of killed *S. aureus*, *P*, was calculated from the reduced CFU counts

23

relative to that in the blank control group in HBSS. ANOVA followed by post-hoc Tukey test was applied to quantify statistical significance.

Bacterial proliferation test: Suspended μwebs were pelleted by centrifugation (10^4 xg for 10 min) and resuspended in HBSS to concentrations of 80, 200, 400, and 800 μg mL^{-1}. Next, 100 μL of the suspended μwebs at different concentrations were separately mixed with 100 μL of the diluted bacterial culture (OD=0.02) for bacterial growth curve measurement. As comparison groups, 100 μL of HBSS supplemented with DNA (40, 100, 200, 400 μg mL^{-1}), or histone (40, 100, 200, 400 μg mL^{-1}) were separately mixed with 100 μL of the diluted bacterial culture and reallocated into 96-well plates (200 μL total in each well). Proliferation of *S. aureus* was monitored at 37°C in a plate reader for 16 hours, and the fluorescence intensity of GFP-*S. aureus* ($E_x/E_m = 488/525$ nm) were measured.

Biofilm characterization: 10^6 *S. aureus* cells were seeded in tissue culture-treated 96-well plates and incubated in a mixture of 100 μL TSBg and 100 μL HBSS added to microwells containing different concentrations of suspended μwebs (0, 50, 75, 100, 200, 300, 500, 750, 1000 μg mL^{-1}) for 24 hours. As control groups, *S. aureus* were separately cultured in a mixture of 100 μL TSBg and 100 μL HBSS supplemented with 0-1000 μg mL^{-1} DNA, or 0-1000 μg mL^{-1} histone under the same condition. Subsequently, the non-attached bacteria in supernatants were extracted and gently transferred to a new 96-well plate, and the remaining biofilms were resuspended in 200 μL HBSS. The non-attached *S. aureus* and the adherent

24

cells in the biofilms were separately quantified by measuring their bacterial fluorescence

(Ex/Em = 488/525 nm) using a plate reader (Biotek Synergy H1). To image the biofilm, *S. aureus* suspensions containing µwebs were seeded onto a silicon wafer in a microplate. The

bacteria deposited on the wafer were fixed and dehydrated before imaging with SEM,

following the protocols described above.

Supporting Information
Supporting Information is available from the Wiley Online Library or from the author.

Conflict of Interest
The authors declare no competing financial interest.

References

[1] a) S. I. Miller, R. M. Tsolis, *Current Opinion in Microbiology*. 2017, **35**, v; b) R. A.

Brady, G. A. O'May, J. G. Leid, M. L. Prior, J. W. Costerton, M. E. Shirtliff, *Infection and*

immunity. 2011, **79**, 1797; c) L. R. Thurlow, M. L. Hanke, T. Fritz, A. Angle, A. Aldrich, S.

H. Williams, I. L. Engebretsen, K. W. Bayles, A. R. Horswill, T. Kielian, *Journal of Immunology*. 2011, **186**, 6585.

[2] S. Sugimoto, F. Sato, R. Miyakawa, A. Chiba, S. Onodera, S. Hori, Y. Mizunoe, *Sci Rep*. 2018, **8**, 2254.

[3] E. Galdiero, L. Lombardi, A. Falanga, G. Libralato, M. Guida, R. Carotenuto, *Pharmaceutics*. 2019, **11**, 322.

[4] K. Schilcher, F. Andreoni, V. Dengler Haunreiter, K. Seidl, B. Hasse, A. S. Zinkernagel, *Antimicrob Agents Chemother*. 2016, **60**, 5957.

[5] A. R. Sultan, T. Hoppenbrouwers, N. A. Lemmens-den Toom, S. V. Snijders, J. W. van Neck, A. Verbon, M. P. M. de Maat, W. J. B. van Wamel, *Infection and Immunity*. 2019, **87**, e00605.

[6] E. van Grinsven, P. H. C. Leliefeld, J. Pillay, C. W. van Aalst, N. Vrisekoop, L. Koenderman, *Journal of Immunological Methods*. 2018, **462**, 83.

[7] F. H. Pilsczek, D. Salina, K. K. H. Poon, C. Fahey, B. G. Yipp, C. D. Sibley, S. M. Robbins, F. H. Y. Green, M. G. Surette, M. Sugai, M. G. Bowden, M. Hussain, K. Zhang, P. Kubes, *Journal of Immunology*. 2010, **185**, 7413.

[8] N. Malachowa, S. D. Kobayashi, B. Freedman, D. W. Dorward, F. R. DeLeo, *The Journal of Immunology*. 2013, **191**, 6022.

[9] T. W. R. Halverson, M. Wilton, K. K. H. Poon, B. Petri, S. Lewenza, *Plos Pathogens*. 2015, **11**, e1004593.

[10] G. Pietrocola, G. Nobile, M. J. Alfeo, T. J. Foster, J. A. Geoghegan, V. De Filippis, P. Speziale, *Journal of Biological Chemistry*. 2019, **294**, 3588.

[11] T. Doolin, H. M. Amir, L. Duong, R. Rosenzweig, L. A. Urban, M. Bosch, A. Pol, S. P. Gross, A. Siryaporn, *Nature Communications*. 2020, **11**, 3888.

[12] M. Rose-Martel, G. Kulshreshtha, N. Ahferom Berhane, J. Jodoin, M. Hincke, *Scientific Reports*. 2017, **7**, 45980.

[13] a) S. C. Davis, C. Ricotti, A. Cazzaniga, E. Welsh, W. H. Eaglstein, P. M. Mertz, *Wound Repair Regen*. 2008, **16**, 23; b) J. Kwiecinski, G. Kahlmeter, T. Jin, *Current Microbiology*. 2015, **70**, 698; c) E. Sweeney, A. M. Lovering, K. E. Bowker, A. P. MacGowan, S. M. Nelson, *Letters in Applied Microbiology*. 2019, **68**, 294.

[14] M. Bhattacharya, E. T. M. Berends, X. Zheng, P. J. Hill, R. Chan, V. J. Torres, D. J. Wozniak, *Infection and Immunity*. 2020, **88**, e00372.

[15] E. T. M. Berends, A. R. Horswill, N. M. Haste, M. Monestier, V. Nizet, M. von Köckritz-Blickwede, *Journal of Innate Immunity*. 2010, **2**, 576.

[16] R. L. Rill, D. K. Oosterhof, *Journal of Biological Chemistry*. 1981, **256**, 12687.

[17] M. Bhattacharya, E. T. M. Berends, R. Chan, E. Schwab, S. Roy, C. K. Sen, V. J. Torres, D. J. Wozniak, *Proceedings of the National Academy of Sciences of the United States of America*. 2018, **115**, 7416.

[18] A. Petretto, M. Bruschi, F. Pratesi, C. Croia, G. Candiano, G. Ghiggeri, P. Migliorini, *PLoS One*. 2019, **14**, e0218946.

[19] Y. Song, U. Kadiyala, P. Weerappuli, J. J. Valdez, S. Yalavarthi, C. Louttit, J. S. Knight, J. J. Moon, D. S. Weiss, J. S. VanEpps, S. Takayama, *Advanced Materials*. 2019, **31**, 1807436.

[20] C. F. Urban, D. Ermert, M. Schmid, U. Abu-Abed, C. Goosmann, W. Nacken, V. Brinkmann, P. R. Jungblut, A. Zychlinsky, *PLOS Pathogens*. 2009, **5**, e1000639.

[21] P. D. Weerappuli, C. Louttit, T. Kojima, L. Brennan, S. Yalavarthi, Y. Xu, L. J. Ochyl, M. L. Maeda, H. S. Kim, J. S. Knight, S. Takayama, J. J. Moon, *Advanced Healthcare Materials*. 2019, **8**, 1900926.

[22]C.-C. Hsu, R.-B. Hsu, R. L. Ohniwa, J.-W. Chen, C.-T. Yuan, J.-S. Chia, C.-J. Jung,

Thrombosis and Haemostasis. 2019, **119**, 786.

[23]a) X.-E. Tan, H.-m. Neoh, M.-L. Looi, S. F. Chin, L. Cui, K. Hiramatsu, S. Hussin, R.

Jamal, *Canadian Journal of Microbiology*. 2017, **63**, 260; b) Y. a. Hyo, b, S. b. Yamada, c,

K. a. Fukutsuji, T. a. Harada, *Medical Molecular Morphology*. 2013, **46**, 217.

[24]a) L. Turnbull, M. Toyofuku, A. L. Hynen, M. Kurosawa, G. Pessi, N. K. Petty, S. R.

Osvath, G. Cárcamo-Oyarce, E. S. Gloag, R. Shimoni, U. Omasits, S. Ito, X. Yap, L. G.

Monahan, R. Cavaliere, C. H. Ahrens, I. G. Charles, N. Nomura, L. Eberl, C. B. Whitchurch,

Nature Communications. 2016, **7**, 11220; b) N. K. Archer, M. J. Mazaitis, J. W. Costerton, J.

G. Leid, M. E. Powers, M. E. Shirtliff, *Virulence*. 2011, **2**, 445.

[25]D. F. Noubouossie, M. F. Whelihan, Y.-B. Yu, E. Sparkenbaugh, R. Pawlinski, D. M.

Monroe, N. S. Key, *Blood*. 2017, **129**, 1021.

[26]a) S. E. Finkel, R. Kolter, *Journal of Bacteriology*. 2001, **183**, 6288; b) A. E. Abaturov,

Theoretical Medicine. 2020, **15**.

[27]V. Dengler, L. Foulston, A. S. DeFrancesco, R. Losick, *Journal of Bacteriology*. 2015,

197, 3779.29

[28] a) U. Eduok, J. Szpunar, E. Ebenso, in *Superhydrophobic Polymer Coatings*, (Eds: S. K. Samal, S. Mohanty, S. K. Nayak), Elsevier, 2019, 245; b) K. Kuroda, K. Okumura, H. Isogai, E. Isogai, *Frontiers in Oncology*. 2015, **5**, 144.

[29]D. Kozon, J. Mierzejewska, T. Kobiela, A. Grochowska, K. Dudnyk, A. Głogowska, A. Sobiepanek, A. Kuźmińska, T. Ciach, E. Augustynowicz-Kopeć, D. Jańczewski, *Macromolecular Bioscience*. 2019, **19**, 1900254.

[30]S. Au - Najmeh, J. Au - Cools-Lartigue, B. Au - Giannias, J. Au - Spicer, L. E. Au - Ferri, *JoVE*. 2015, e52687.

[31]T. Brandt, S. Breitenstein, H. von der Hardt, B. Tümmler, *Thorax*. 1995, **50**, 880.

[32]a) R. Gray, B. McCullagh, P. McCray, Antibiotics. 2015, 62; b) B. Rada, *Communicative & integrative biology*. 2017, **10**, e1296610.

[33]N. Yamamoto, M. Ojima, S. Hamaguchi, T. Hirose, R. Takegawa, N. Matsumoto, T. Irisawa, M. Seki, O. Tasaki, T. Shimazu, K. Tomono, *Critical Care*. 2015, **19**, 77.

[34]Kong, T., Luo, G., Zhao, Y., Liu, Z., *Advanced Functional Materials*. 2019, **29**, 1808012.

[35]Jinlong Yu, Feiyang Zhang, Yunqi Pan, Jianqiang Wang, Pei Han, Jin Tang, Hao Shen, *Frontiers in microbiology*. 2020, **11**, 587175.

[36]T. D. Read, R. A. Petit, 3rd, Z. Yin, T. Montgomery, M. C. McNulty, M. Z. David, *BMC microbiology*. 2018, **18**, 206.
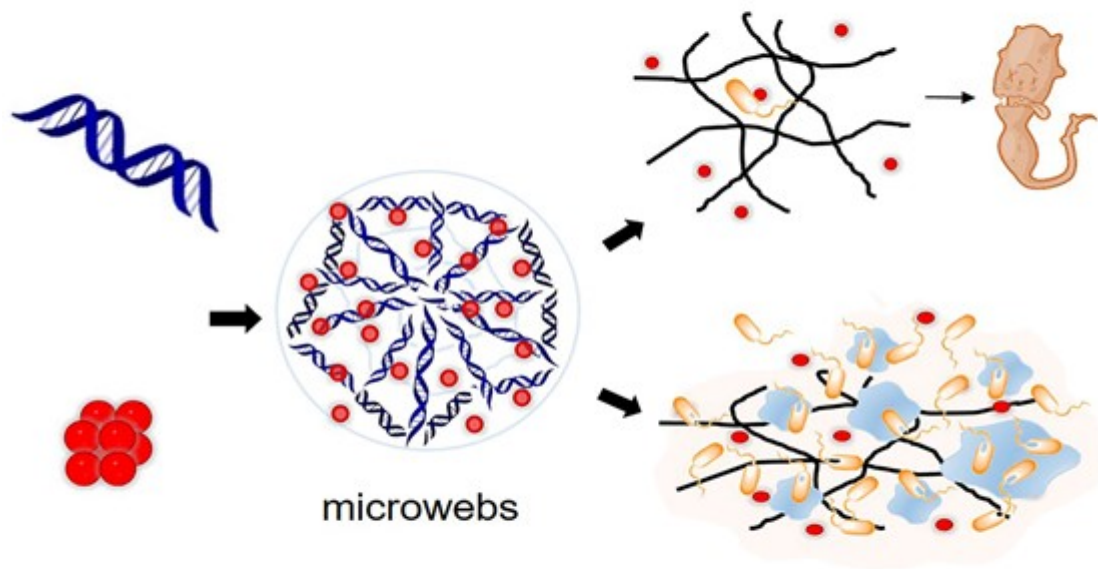
[37]J. Chi, Q. Ma, Z. Shen, C. Ma, W. Zhu, S. Han, Y. Liang, J. Cao, Y. Sun, *Nanoscale*. 2020, **12**, 11008.

[38]T. Yang, H. Pan, J. He, Z. Gai, X. Cao, *Process Biochemistry*. 2019, **79**, 185.

ToC text

'Microwebs', a web-like DNA structure mimicking the neutrophil extracellular traps shows antimicrobial activity against S. aureus at physiological conditions, but it paradoxically induces biofilm formation at higher concentrations. This paradigm can be explained under the framework of electrostatic interactions between DNA, histone and bacterial cell walls, which provides a materials-based insight for understanding the NETs-relevant pathology in the biofilm disease.

ToC figure

microwebs

Author I